Exploring Deep Learning for Air Pollutant Emission Estimation

Lin Huang,[★,1] Song Liu,[★,2,3] Zeyuan Yang,[4] Jia Xing,[2,3] Jia Zhang,[1] Jiang Bian,[1] Siwei Li,[5,6] Shovan Kumar Sahu,[2,3] Shuxiao Wang,[2,3] Tie-Yan Liu[1]

[1]Microsoft Research, Beijing, China
[2]State Key Joint Laboratory of Environmental Simulation and Pollution Control, School of Environment, Tsinghua University, Beijing, China
[3]State Environmental Protection Key Laboratory of Sources and Control of Air Pollution Complex, Beijing, China
[4]School of Economics and Management, Tsinghua University, Beijing, China
[5]School of Remote Sensing and Information Engineering, Wuhan University, Wuhan, China
[6]State Key Laboratory of Information Engineering in Surveying, Mapping and Remote Sensing, Wuhan University, Wuhan, China
[★]These authors contributed equally to this work.

Correspondence to: Jia Xing (xingjia@tsinghua.edu.cn); Jia Zhang (zhangjia@microsoft.com)

Abstract. The inaccuracy of anthropogenic emission inventory on a high-resolution scale due to insufficient basic data is one of the major reasons for the deviation between air quality model and observation results. A bottom-up approach, as a typical emission inventory estimation approach, requires a lot of human labor and material resources, and a top-down approach focuses on individual pollutants that can be measured directly and relies heavily on traditional numerical modelling. Lately, deep neural network has achieved rapid development due to its high efficiency and non-linear expression ability. In this study, we proposed a novel method to model the dual relationship between emission inventory and pollution concentration for emission inventory estimation. Specifically, we utilized a neural network based comprehensive chemical transport model (NN-CTM) to learn the complex correlation between emission and air pollution. We further updated the emission inventory based on backpropagating the gradient of the loss function measuring the deviation between NN-CTM and observations from surface monitors. We first mimicked the CTM model with neural networks (NN) and achieved a relatively good representation of CTM with similarity reaching 95%. To reduce the gap between CTM and observations, the NN model would suggest an updated emission of NO_x, NH_3, SO_2, VOC and primary $PM_{2.5}$ which changes by -1.34%, -2.65%, -11.66%, -19.19% and 3.51%, respectively, on average of China in 2015. Such ratios of NO_x and $PM_{2.5}$ are even higher (~10%) particularly in Northwest China where suffers from large uncertainties in original emissions. The updated emission inventory can improve model performance and make it closer to observations. The mean absolute error for NO_2, SO_2, O_3 and $PM_{2.5}$ concentrations are reduced significantly by about 10%~20%, indicating the high feasibility of NN-CTM in terms of significantly improving both the accuracy of emission inventory as well as the performance of air quality model.

1 Introduction

The clean air policies have been implemented by China government since 2010 which has been effectively reducing the pollutant concentrations such as sulfur dioxide (SO_2), nitrogen oxides (NO_x) (Zheng et al., 2018). Nevertheless, China still faces challenges in addressing O_3 and $PM_{2.5}$ pollutions. Particularly, the level of ozone (O_3) in China has increased by 1.3% from 2013 to 2017 (Li, 2019); moreover, concentrations of $PM_{2.5}$ (particulate matter with an aerodynamic diameter less than 2.5 μm) in most Chinese cities still far exceed the World Health Organization (WHO) recommended values (<10 μgm^{-3}), leading to frequent heavy pollution events (Guo et al., 2014; Richter et al., 2005; Vesilind et al., 1988). Such high pollutant concentration may substantially affect human health given air pollution has being ranked fifth in global risk factors for mortality (Institute, 2019).

A prerequisite of effectively controlling air pollution lies in accurate knowledge of the related emission sources. A well-established emission inventory should summarize the amount of pollutants emitted into atmosphere from all sources in a specific region and time span (Institute, 2019). A typical bottom-up approach is adopted to develop the emission inventory through investigation of emission sources in Air Benefit and Cost and Attainment Assessment System Emission Inventory (ABaCAS-EI) (Zheng et al., 2019) and Multi-resolution Emission Inventory (MEIC) (He, 2012) developed by Tsinghua University, wherein the activity rate of each source is multiplied with emission factor (Vallero and Daniel, 2018). Such technology-oriented bottom-up emission inventory can reflect the types of technology operated in China but has limitation in actual application because of its need for labor power and material resources, especially in cities where it is hard to support thorough investigation (Xing et al., 2020b). What's more, varied assumptions for activity rate and emission factor from different studies result in large uncertainties (Aardenne and Pulles, 2002). Therefore, the development of a method for efficient, low-cost, and sufficiently accurate grid-emission information is being considered.

The top-down method, as another typical emission inventory estimation approach, can be used to constrain emission estimation by combining observation results from surface monitors and satellite retrievals. Brioude et al. (2012) has estimated emissions of anthropogenic CO, NO_x and CO_2 in the Los Angeles Basin using the FLEXPART Lagrangian particle dispersion model based on the top-down method. Recently, Yang et al. (2021) linked the bottom-up MAPLE model with the top-down CGE model to evaluate deep decarbonization pathways' (DDP) comprehensive impacts in China. However, most of previous studies merely focused on individual pollutants that can be measured directly (Brioude et al., 2012; Xing et al., 2020a; Yang et al., 2021) and relied on traditional numerical modelling.

On the contrary, neural networks (NN), as a more efficient tool, can also model complex nonlinear relations in the atmospheric system thus converting precursor emissions into ambient concentrations. Due to its ability of end-to-end learning, NN can automatically extract key features of input data and capture the behaviour of target data, thus has been widely used in atmospheric science recently (Fan et al., 2017; Tao et al., 2019; Wen et al., 2019; Xing et al., 2020a; Xing et al., 2020c). For example, many studies (Fan et al., 2017; Tao et al., 2019; Wen et al., 2019) combined recurrent NN (RNN) and convolutional NN (CNN) to capture spatial and temporal features in air pollution related questions since RNN has a strong capability in

mining temporal patterns from time series data (Cho et al., 2014; Chung et al., 2014; Hochreiter and Schmidhuber, 1997) with
certain ability to handle missing values efficiently (Fan et al., 2017) and CNN exhibits potentials in leveraging spatial
dependencies, e.g., in meteorological prediction (Krizhevsky et al., 2012). Furthermore, Xing et al. (2020d) applied NN to the
surface response model (RSM), thus significantly enhancing the computational efficiency, demonstrating the utility of deep
learning approaches for capturing the nonlinearity of atmospheric chemistry and physics. The application of deep learning
improves the efficiency of air quality simulation and can quickly provide data support for the formulation of emission control
policies, so as to adapt to the dynamic pollution situation and international situation. But the use of deep NN to estimate
emission inventory is more complex compared to traditional machine learning problems, because there is no precise emission
observation that can be used as supervision for model training.

To address all these issues, we proposed a novel method based on dual learning (He et al., 2016), which leverages the primal-
dual structure of artificial intelligence (AI) tasks to obtain informative feedbacks and regularization signals, thus enhancing
both the learning and inference process. In terms of emission inventory estimation, if we have a precise relationship from
emission inventory to pollution concentrations, we can use the pollution concentrations as a constraint to get accurate emission
inventory. In particular, we proposed to employ a neural network based chemical transport model (NN-CTM) with a delicately
designed architecture, which is *efficient* and *differentiable* compared to the chemical transport model (CTM). Furthermore,
when a well-trained NN-CTM can accurately reflect the *direct* and *indirect* physical and chemical reactions between emission
inventory and pollutant concentrations, the emission inventory can be updated by backpropagating the gradient of the error
between observed and NN-CTM predicted pollutant concentrations. Figure 1 shows the framework of this study.

The method used for this study is described in Section 2. Section 3 takes China emission inventory estimation as an example
to demonstrate the superiority of our method. In section 4, we make a conclusion and discuss some possible future work.
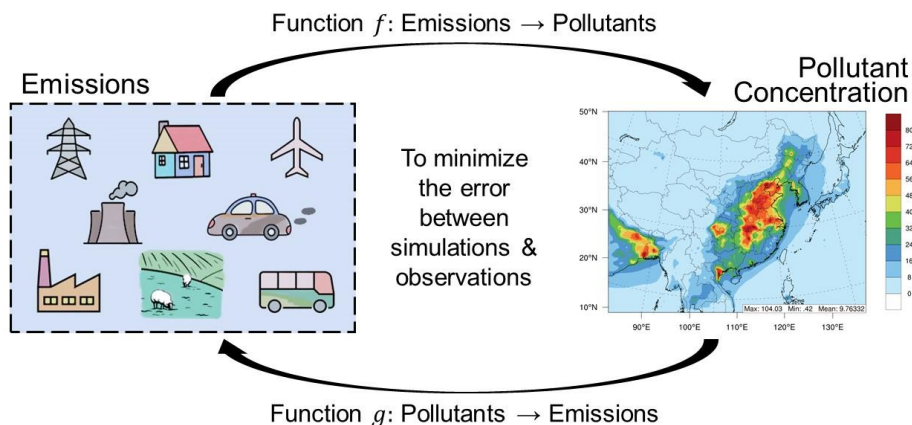
Figure 1: Framework of this study.

2.Method

2.1 Main Framework

90 The task of emission inventory estimation can be naturally formalized into a typical dual learning framework. Concretely, we denote x_t as the data of emission volumes and meteorological conditions and y_t as the corresponding pollutant concentration at time t. In addition, we denote the mapping function from emission to pollutant concentration as f and that from pollutant concentration to emission as g. Since the transformation from emission to pollutant concentration is a continuous process in time, approximately, we have the following equations:

95 $$y_t = f(x[(t - k + 1):t]),\qquad(1)$$

$$x_t = g(y[(t - k + 1):t]),\qquad(2)$$

where $x[i:j]$ is defined as $\{x_i, x_{i+1}, \dots, x_j\}$ for convenience, so is $y[i:j]$.

The formulas above are based on two assumptions:

1.   The pollutant concentration is only dependent on the emission and meteorological conditions in the past k time steps,
100 e.g., hours or days.

2.   There is a bijection relationship between emission and pollutant concentration. This is a necessary prerequisite for the existence of function g.

The first assumption will hold true as long as setting a sufficiently large k. The second assumption may not be true unless we introduce more external constraints on emission inventory, since there exists information loss in the process from emission to
105 pollutant concentration.
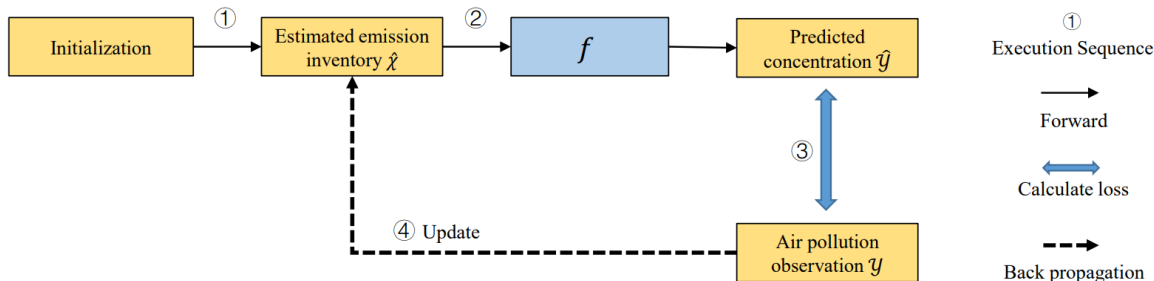
Figure 2: The whole process of emission inventory estimation.

In fact, it is quite difficult to learn the function g directly without emission observations as supervision. Hence, we employ dual learning framework to learn function g indirectly through leveraging function f. The framework of this process is illustrated in Figure 2. In particular, the whole process of emission inventory estimation includes the following steps:

1. Use the existing emission inventory which is still not accurate enough as the initial emission data $\hat{\mathcal{X}}$.

2. Given $\hat{\mathcal{X}}$, calculate the corresponding predicted pollutant concentration data $\hat{\mathcal{Y}}$.

3. Calculate the loss between the observed values of pollutants $\mathcal{Y}$ and the predicted pollutant concentrations $\hat{\mathcal{Y}}$.

4. Adjust the estimated emission inventory $\hat{\mathcal{X}}$ by backpropagating the gradient of the loss based on function f.

5. Repeat steps 2-4 until achieving sufficient accuracy for predicted concentration.

Although the chemical transport model (CTM) system can handle the transition from emission to pollutant concentration, it is not differentiable, which makes it quite hard to update emission inventory through backpropagation algorithm in the dual learning framework. In order to establish a differentiable CTM, we propose to build a neural network based chemical transport model (NN-CTM) as the system approximation. More details will be described in the following subsections.

2.2 Deep Neural Network based Chemical Transition Model Approximation

Pollutant concentration is usually estimated using CTM which uses emission inventory as input. In the dual learning framework, this input will be updated in turn based on observed concentrations through the backpropagation algorithm. This requires the CTM to be differentiable. To this end, we propose to use deep neural networks to approximate the CTM system. Concretely, to learn this neural network based chemical transport model (NN-CTM), we apply a supervised learning approach that leverages the training data whose input is the same as that of CTM and corresponding label is the output of CTM. The whole architecture is shown in Figure 3.
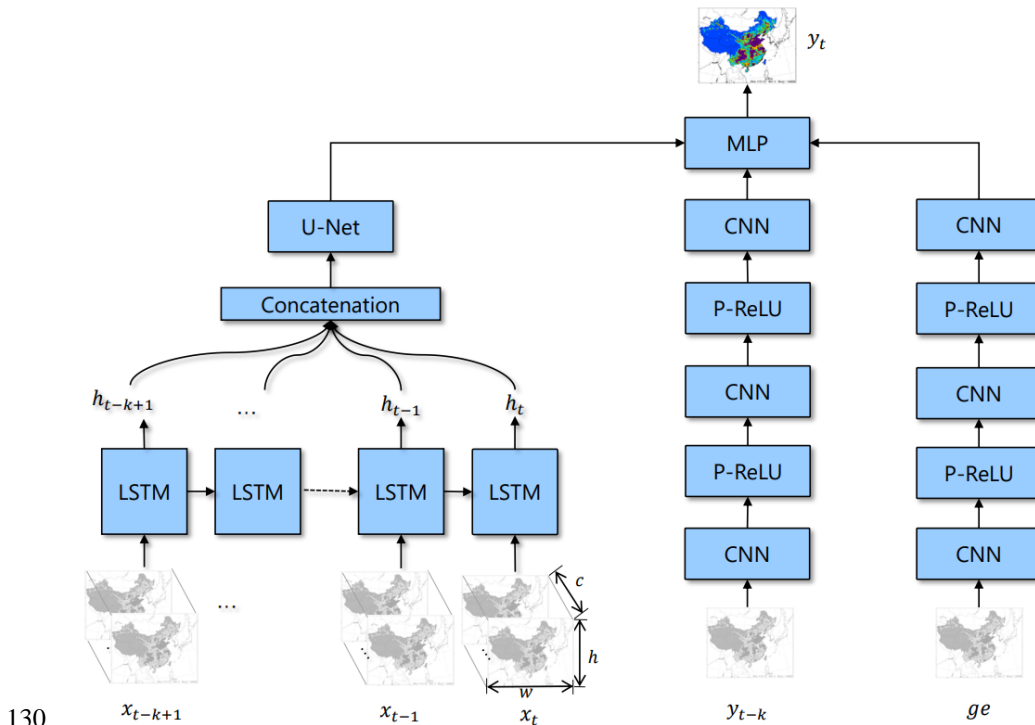
Figure 3: NN-CTM structure. c **represents channel, which consists of emission inventory and meteorological data.** h, w **represent the height, width of input.** ge **is geographic information. We employ long short term memory (LSTM) to capture the temporal information, and U-Net to capture the spatial information. CNN represents convolution network. P-ReLU (He et al., 2015b) is a nonlinear activation function. MLP means multiple layers of perceptrons with threshold activation. The model structure is also named as LSTM-U-Net.**

The input data of our NN-CTM are similar to that of CTM, including emission inventory, meteorology and geographical data. The first two are time-dependent data, while the last one, denoted as ge, is static data. In the Eulerian grid based CTM system, for each time step t, the dynamic input data x_t is a matrix with dimension $w \times h \times c$. The concentration is simulated continuously in a continuous time sequence. Unlike CTM, the NN-CTM cannot deal with too long data sequences. Thus, we just use the data from past k time steps (i.e, $x[t-k+1:t]$) as input for the pollutant concentration estimation y_t. At the same time, we add y_{t-k} as supplementary input data into the network. Same as CTM, the output y_t of NN-CTM is a matrix with dimension $w \times h \times l$, where l is the number of concerned pollutant species.

The NN-CTM consists of three branches: two CNN branches for y_{t-k} and ge, and one long short term memory (LSTM) (Hochreiter and Schmidhuber, 1997) with U-Net (Ronneberger et al., 2015) branch. The CNN branches are used to extract features for y_{t-k} and geographical information. We employ parametric rectified linear unit (P-RELU) (He et al., 2015b) as the non-linear activation function in these branches to improve model fitting with nearly zero extra computational cost and little overfitting risk. We adopt the architecture of combining LSTM and U-Net based on the understanding of temporal-spatial relationship in emission inventory. In temporal dimension, pollutants are the accumulation of historical emissions. In spatial

150 dimension, adjacent grids will affect each other because of meteorological and diffusion factors. The LSTM layer is used to aggregate information from time series data $x[t-k+1:t]$. The aggregated sequence of hidden states $h_{t-k+1},\dots,h_t$ will be concatenated and entered into U-Net block. U-Net is a widely adopted pixel-to-pixel model which can effectively utilize neighbour information. In U-Net, the stacked of convolution can get the neighbour information with a bigger receptive field (e.g. stacking 5×5 convolution and 5×5 convolution can get a 9×9 convolution), the non-linear function (P-RELU) is

155 employed to improve model fitting with nearly zero extra computational cost and little overfitting risk, and the batch normalization and dropout are employed to enhance the robustness of the model. We calculate that the receptive field of our model is 38×38 grid. In other words, the predicted pollutant concentration is related to its surrounding 38×38 grid's information, which represents the transmission between different grids. Meanwhile, the closer the distance, the greater the contribution. We employ 2-layers U-Net as shown in Figure 4 to capture the spatial information between grids.

160
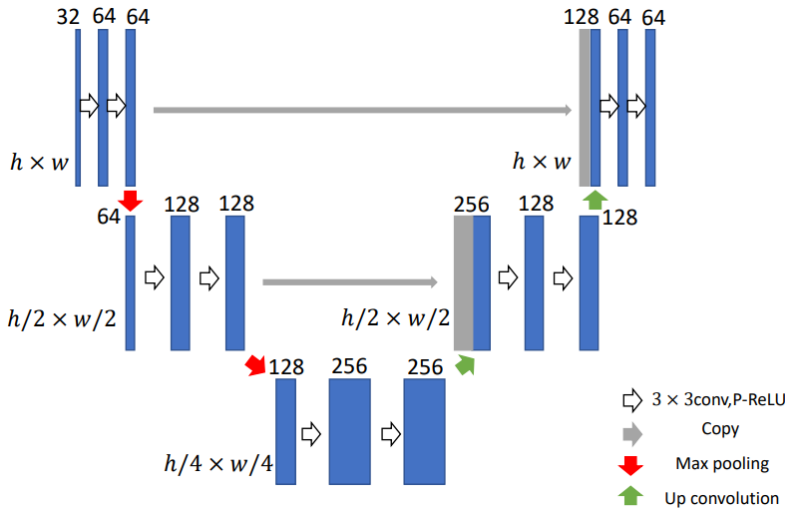
Figure 4: U-Net structure (2-layers). The model structure yields a u-shaped architecture. 3×3 conv is a convolution (Huang et al., 2016) function. P-ReLU (Huang et al., 2016) is a nonlinear activation function. Max pooling is a down sample function. Up convolution (Zeiler et al., 2010) is a deconvolution function, which is also named as up sample function.

165

In the training process, we take $(\mathcal{X}_{CTM}, \mathcal{Y}_{CTM})$ as training dataset, where $\mathcal{X}_{CTM}$ is the input data of the CTM system while $\mathcal{Y}_{CTM}$ is the corresponding output. Since relative changes in pollutant concentrations are the metric often used by policymakers, we adopt an objective function that measures the relative loss between NN-CTM predicted and CTM-simulated pollutant concentrations. We denote the output of NN-CTM as $\hat{\mathcal{Y}}_{NN}$, and have:

170
$$L(\hat{\mathcal{Y}}_{NN}, \mathcal{Y}_{CTM}) = \frac{1}{Nhwl}\sum_{n=1}^{N}\sum_{i,j,c}\left(|\hat{y}_{i,j,c}^{(n)} - y_{i,j,c}^{(n)}|\right), \tag{3}$$

$$g_w = \frac{\partial L(\hat{\mathcal{Y}}_{NN}, \mathcal{Y}_{CTM})}{\partial w}, \tag{4}$$

where N is the number of samples, $i \in [1, h]$, $j \in [1, w]$ and $c \in [1, l]$, and $y_{i,j,c}^{(n)}$ represents the concentration of pollutant c-th in grid with location (i, j) in the n-th sample. The parameters of NN-CTM will be updated based on the gradients given by g_w, and the Adaptive Moment (Adam) estimation (Kingma and Ba, 2014) is used as optimizer.

175 *Model robustness.* We ensure the robustness of the model from three aspects: 1) Model structure. Inspired by computer vision tasks, we adopt the batch-normalization (Ioffe and Szegedy, 2015), dropout (Srivastava et al., 2014), L2 regularization (Zhang et al., 2016) to improve the generalization and robustness. 2) Early stop. When we train the NN-CTM, we split the data into train dataset and validation dataset, and we stop the model training when the evaluation in validation dataset does not improve within 1000 iterations. 3) Data augmentation. During training, we employ the noise injection, random rescaling, random

180 rotation method to avoid the overfitting in training dataset.

2.3 Emission Inventory Estimation Based On NN-CTM

Given a well-trained NN-CTM whose approximation accuracy is high enough for predicting pollutant concentrations, the emission inventory can be updated based on the error between observed and NN-CTM predicted pollutant concentrations. The observation data will help update the surrounding grids' emission inventory within the receptive field. However, in extreme

185 circumstances, if we have no observation data, our method will not work as we have no more information to adjust the emission inventory. If the observation data is denser, the emission inventory estimation is more accurate as it can consider more observation data.

In particular, we make the relationship between emission and pollutant concentration more robust by fixing the trained LSTM-U-Net model parameter. Then by training NN-CTM parameter, we adjust the input emission inventory to minimize the loss

190 between NN-CTM output and observation. Such loss can be formally defined as:

$$L(\hat{\mathcal{Y}}_{NN}, \mathcal{Y}_{obs}^*) = \frac{1}{Nhwl} \sum_{n=1}^{N} \sum_{i,j,c} M_{i,j}(|\hat{y}_{i,j,c}^{(n)} - y_{i,j,c}^{*(n)}|) , \tag{5}$$

$$g_e = \frac{\partial L(\hat{\mathcal{Y}}_{NN}, \mathcal{Y}_{obs}^*)}{\partial e} , \tag{6}$$

where $\mathcal{Y}_{obs}^*$ represents observed pollutant concentration (we use average value in case of multiple observation stations in a grid), $M_{i,j}$ is a binary indicator variable indicating whether or not there is a site monitoring equipment in grid (i, j). The

195 emission inventory will be updated by backpropagating the gradient g_e. The stochastic gradient descent (SGD) method (Bottou, 2010) is used as optimizer.

Meanwhile, aiming at ensuring the reasonableness and effectiveness of estimated emission inventory, we set two constrains: 1) The update rate of emission inventory to be a maximum of 200% compared with the prior emission for each grid. There exist biases in meteorological conditions and chemical mechanism, which determines that we cannot attribute all the errors to

200 the emission inventory. If the update ratio is very large, the NN-CTM cannot well reflect the correlation of the unseen data.

Furthermore, the prior emission is accurate to a certain extent in terms of the spatial and temporal dimensions. 2)The updated emission inventory must be positive.

3. Experiments and Results Analysis

In this section, we apply our proposed method for emission inventory estimation in China in 2015. In the following, we will first describe the data and CTM configuration. After that, we will show experimental results in terms of the accuracy of NN-CTM. Then, we conduct further analysis on the prior emission inventory and our emission inventory estimation results.

3.1 Data and CTM Configuration

The prior emission inventory ABaCAS-EI with high spatial and temporal resolution is based on the bottom-up method, including primary pollutants such as NO_x, ammonia (NH_3), SO_2, volatile organic compounds (VOC) and primary $PM_{2.5}$. ABaCAS-EI is a grid-unit-based emission inventory including sources of power, cement, steel industries, and mobile sources. It also takes into consideration of technical progress and more stringent emission standards (Zheng et al., 2019). The prior emission inventory is initially used for NN-CTM training and then updated as per the proposed method of dual learning.

Geographical data is a fixed attribute of one grid, like land type, mountains, depressions or elevation, etc. and in this study is obtained from the Moderate Resolution Imaging Spectroradiometer (MODIS) with 15s resolution (Friedl et al., 2002). Meteorological conditions are simulated from the Weather Research and Forecasting model (WRF, version 3.7). WRF configuration includes Morrison microphysics scheme (Morrison et al., 2009), RRGM radiation scheme (Mlawer et al., 1998; Mlawer et al., 1997), Pleim-Xiu land surface scheme (Pleim and Xiu, 1995; Xiu and Pleim, 2001), ACM2 planetary boundary layer (PBL) physics scheme (Pleim, 2007) and Kain-Fritsch cumulus cloud parameterization (Kain, 2004), which matches our previous studies (Ghil and Malanotte-Rizzoli, 1991; Wikle, 2003). Data assimilation is adopted in WRF simulations based on observation data for the upper air and surface from National Centers for Environmental Prediction (NCEP) datasets. The simulated temperature, humidity, wind speed and direction have good agreement with the observations from the National Climatic Data Center (NCDC, https://www.ncdc.noaa.gov/data-access/land-based-station-data/) (Ding et al., 2019; Liu et al., 2019; Zhao et al., 2013).

The Community Multiscale Air Quality Model (CMAQ, version 5.2) configured with the AERO6 aerosol module (Appel et al., 2013) and the Carbon Bond 6 (CB6) gas-phase chemical mechanism (Sarwar et al., 2008) is chosen as the representative CTM to simulate pollutant concentrations (Appel et al., 2018; Byun, 1999). Hourly observation data for air pollution (including SO_2, NO_2, O_3 and $PM_{2.5}$) is obtained from the China National Environmental Monitoring Centre (http://beijingair.sinaapp.com/), which are used for adjusting emission inventory.

The simulation domain covers mainland China and portions of surrounding countries with a 27km × 27km horizontal resolution (with $h = 182$ and $w = 232$) and 14 vertical layers from ground to 100 hPa. Simulations are performed in January,

April, July, and October 2015 to represent winter, spring, summer, and autumn, respectively. A 5-day simulation spin-up was performed to minimize the effects of initial conditions. Pollutant concentrations are analysed at monthly averages.

3.2 NN-CTM Learning and Evaluation

Training parameters. The parameter of NN-CTM was optimized using Adam optimizer with a mini-batch size of 8. A learning
235 rate of 0.001 was used. To reduce the risk of over-fitting, we applied weight regularization on all trainable parameters during training and fine-tuning. The NN-CTM was trained for 30000 epochs.

Metrics. Model performance was evaluated using mean absolute error (MAE) calculated using the following equation:

$$L\big(\hat{\mathcal{Y}}_{NN}, \mathcal{Y}_{CTM}\big) = \frac{1}{Nhwl}\Sigma_{n,i,j,c}\big(|\hat{y}_{i,j,c}^{(n)} - y_{i,j,c}^{(n)}|\big)\,, \tag{7}$$

Where N, h, w, l are the number of samples, height, width and the number of observed pollutants in each grid, respectively,
240 further $n \in [1, N], i \in [1, h], j \in [1, w]$ and $c \in [1, l]$.

Evaluation. We examined the performance of NN-CTM to check whether it has learnt the relationship between emission and pollutant concentration.

We trained NN-CTM on the data of first 22 days in January, April, July and October 2015 and tested it on the remaining successive 8 days of each month. As listed in Table 1, NN-CTM (with LSTM-U-Net) can well reproduce the spatial and
245 temporal relation with a small MAE of 0.27, 0.17, 1.39 ppbv and 1.46 $\mu g\,m^{-3}$ for NO_2, SO_2, O_3 and $PM_{2.5}$, respectively, on average of four months. Results suggest that the NN-CTM can well reproduce the CTM within an acceptable bias, thus can be used for emission adjustment. Such bias (<4%) is much smaller than that of simulation compared to observations which are normally more than 10% even 20%.

250 **Table 1: Evaluation of NN-CTM simulation in China (mean absolute error between CTM and NN-CTM). LSTM-U-Net is our proposed method. And then, to compare the model performance, we select another professional deep neural network method residual network (ResNet) (He et al., 2015a).**

Model	NN-CTM (with LSTM-U-Net)				NN-CTM (with ResNet)			
Variables	$PM_{2.5}$ ($\mu g\,m^{-3}$)	O_3 (ppbv)	NO_2 (ppbv)	SO_2 (ppbv)	$PM_{2.5}$ ($\mu g\,m^{-3}$)	O_3 (ppbv)	NO_2 (ppbv)	SO_2 (ppbv)
Jan.	1.65	1.39	0.34	0.25	1.65	1.44	0.36	0.26
Ari.	1.74	1.46	0.25	0.16	1.73	1.64	0.26	0.18
Jul.	1.04	1.38	0.23	0.12	1	1.45	0.25	0.13
Oct.	1.43	1.34	0.27	0.16	1.53	1.44	0.29	0.17
Average	1.46	1.39	0.27	0.17	1.48	1.49	0.29	0.19
Error (Unit: %)	3.6	3.9	1.9	2.2	3.7	4.3	2.1	2.5

In order to further verify the superiority of our model architecture, we employed the ResNet (He et al., 2015a), another widely
255 adopted deep NN method in image processing. Compared to ResNet, the performance of NN-CTM (with LSTM-U-Net) was
superior, with improved MAE of 0.02, 0.02, 0.10 ppbv and 0.02 μg m^{-3} for NO_2, SO_2, O_3 and $PM_{2.5}$, respectively, on average
of four months, as listed in Table 1.

3.3 Emission Inventory Updating and Analysis

A well trained NN-CTM is used to update the emission inventory through back propagation using stochastic gradient descent
260 SGD (Bottou, 2010) optimizer with a mini-batch size of 2. The learning rate is 0.1. The optimization of emissions is achieved
after 10000 epochs.
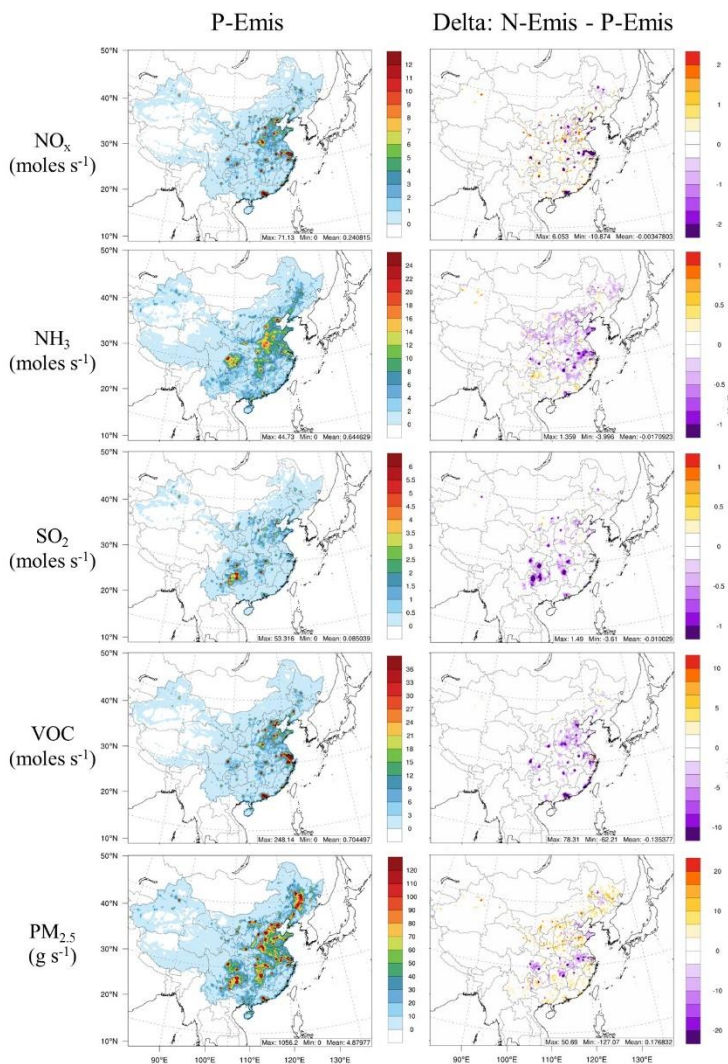
Figure 5: Emission rates of NO$_x$, NH$_3$, SO$_2$, VOC and primary PM$_{2.5}$ in P-Emis and their changes in N-Emis.

265

For convenience, we denote the emission inventory from ABaCAS-EI as prior emissions (P-Emis) and the updated emission inventory as NN-emission (N-Emis), which is constrained by station observations. Compared with P-Emis, N-Emis has adjusted emission rates of NO$_x$, NH$_3$, SO$_2$, VOC and primary PM$_{2.5}$ as per the difference between simulated concentrations and the observed values of pollutants in each grid, as shown in Figure 5. Average emission rates of NH$_3$, SO$_2$ and VOC in

270 most grids tend to decrease, while that of primary PM$_{2.5}$ tend to increase except for in the Yangtze River Basin, which may be related to the non-included dust emission. Changes in emission rate of NO$_x$ vary a lot by region, and such changes are concentrated in urban areas. The distribution of N-Emis for each grid is consistent with P-Emis, indicating that the deep

learning method in this study can identify the distribution of emission sources and focus on the calibration in high-emission areas.

275 Annual anthropogenic emissions in China for NO_x, NH_3, SO_2, VOC and primary $PM_{2.5}$ in P-Emis are 20.44, 10.39, 14.40, 23.05 and 7.19 Mt, respectively (Liu et al., 2020), while in N-Emis changed by -1.34%, -2.65%, -11.66%, -19.19% and 3.51%, respectively.

Table 2: Change ratios of N-Emis compared with P-Emis in four months. Unit: %.

Month	Variables				
	NO_x	NH_3	SO_2	VOC	$PM_{2.5}$
Jan.	3.72	1.88	-12.38	-25.36	4.64
Apr.	-1.49	-2.56	-8.96	-18.27	4.69
Jul.	-11.68	-2.29	-11.42	-12.8	1.8
Oct.	3.6	-4.61	-13.32	-19.03	2.4
Average	-1.34	-2.65	-11.66	-19.19	3.51

280

The sensitivity of change ratios to different seasons varies. Table 2 lists the change ratios of N-Emis compared to P-Emis in four months. As for N-Emis, NO_x increases in January and October by about 3.5~4.0%, while it decreases by more than 10% in July. Emission of NH_3 increases in January while decreases in other three months with the highest decrease registered in October. Emission of SO_2 tends to decrease in all four months with ratios around 10%. Emission of VOC also tends to decrease

285 but with a larger magnitude of about 20% compared to SO_2, which may be related to the overestimation of O_3. Emission of primary $PM_{2.5}$ tends to increase by less than 5% in four months.

Such changes in emissions are based on mathematical algorithms and thus cannot be explained by physical and chemical processes. The NN method tries to give a solution to make simulation results of all pollutant species closer to observations by compensating the errors in emission inventory. For example, concentrations of $PM_{2.5}$ obtained using P-Emis are generally

290 lower than the observed level, so the emission of primary $PM_{2.5}$ will be increased during the adjustment. SO_2 tends to be overestimated using P-Emis, so the adjustment tends to decrease. However, because sulfate is an important component of $PM_{2.5}$, the adjustment of SO_2 will be restricted by the underestimation of $PM_{2.5}$. Concentrations of O_3 obtained using P-Emis are generally higher than the observed level, so it tends to reduce the emissions of NO_x and VOC, which are precursors of O_3, during the adjustment. It is worth noting that the adjustment range of NO_x is much lower than of VOC, because only the

295 observed concentration of NO_2 is used as a constraint. Such results are consistent with our previous study (Xing et al., 2020a). In order to further analyse the change of emissions at a regional level, we calculated the four-month average emissions of P-Emis and change ratios of N-Emis for five emission species in the Beijing-Tianjin-Hebei region (BTH), the Yangtze River Delta (YRD), the Pearl River Delta (PRD), the Sichuan Basin (SCH) and northwest China (NWC), as highlighted in Figure 6.

The first four areas were selected because they are the main population clusters, and NWC was selected because there are so few observation sites in this area that the constraints are relatively insufficient.

Variable	P-Emis	N-Emis (%)
NO_x	9.48	14.02
NH_3	41.38	-0.32
SO_2	23.35	2.77
VOC	0.05	-2.43
$PM_{2.5}$	0.80	8.91

Variable	P-Emis	N-Emis (%)
NO_x	56.43	1.13
NH_3	68.51	-3.32
SO_2	48.73	-24.69
VOC	0.49	-20.13
$PM_{2.5}$	2.68	-0.1

Variable	P-Emis	N-Emis (%)
NO_x	41.12	-4.55
NH_3	143.84	-1.49
SO_2	123.32	-24.22
VOC	0.22	-29.68
$PM_{2.5}$	2.37	-5.95

Variable	P-Emis	N-Emis (%)
NO_x	69.96	-14.73
NH_3	70.91	-2.73
SO_2	36.89	-4.99
VOC	0.91	12.54
$PM_{2.5}$	2.32	-1.14

Variable	NO_x	NH_3	SO_2	VOC	$PM_{2.5}$
P-Emis	36.50	52.19	21.23	0.24	1.07
N-Emis (%)	-5.42	0.03	-16.74	-26.23	7.12

Figure 6: Five typical regions of China : Beijing-Tianjin-Hebei region (denoted as BTH), the Yangtze River Delta (denoted as YRD, covering Jiangsu, Zhejiang and Shanghai), the Pearl River Delta (denoted as PRD, covering Guangdong), the Sichuan Basin (denoted as SCH, covering Sichuan and Chongqing) and northwest China (denoted as NWC, covering Xinjiang), and their month-average emissions of four months in P-Emis (with unit of kt except for VOC with Mmol) and change ratios in N-Emis (with unit of %).

The adjustment of emission varies greatly by seasons and regions. Seasonal details are listed in Table 3. The four-month average changes of N-Emis in BTH are highest for SO_2 and VOC emissions reaching about -20% while that of NO_x, NH_3 and primary $PM_{2.5}$ vary by less than 5%. In YRD, NOx and VOC emissions record the highest extent of changes with -14.73% for NO_x and 12.54% for VOC. The range of changes in other emission species is less than 5% (all decrease). Emission of primary $PM_{2.5}$ in PRD increases by about 7%, which is the largest change ratio among four urban regions. Emission of NH_3 in PRD changes the least compared with other regions. In SCH, emissions of SO_2 and VOC decrease the most (change ratio) compared with other emission species (>20%). Emission of primary $PM_{2.5}$ in SCH, which decreases by 5.95%, shows an opposite trend to that in PRD. As for in NWC, emissions of NH_3 and VOC show a small decrease (<5%), while emissions of NO_x and primary $PM_{2.5}$ have a large percentage increase compared with other regions (10%), thus particularly indicating the large inaccuracy in emission inventory in NWC.

Table 3: Emissions and change ratios in five typical regions of four months.

Month	Variables	Version	Regions				
			BTH	YRD	PRD	SCH	NWC

Jan.	NO$_x$	P-Emis (kt)	68.05	70.56	37.07	43.29	10.26
		N-Emis (%)	-7.19	6.24	4.55	2.65	8.74
	NH$_3$	P-Emis (kt)	28.65	24.42	6.5	24.84	5.52
		N-Emis (%)	0.67	0.59	8.3	5.13	8.64
	SO$_2$	P-Emis (kt)	90.13	40.16	21.72	150.67	34.06
		N-Emis (%)	-11.93	-11.38	-13.92	-26.14	-1.5
	VOC	P-Emis (Mmol)	0.81	0.99	0.25	0.28	0.05
		N-Emis (%)	-5.53	-12.73	-37.52	-36.39	2.61
	PM$_{2.5}$	P-Emis (kt)	4.66	2.22	1.14	3.6	0.85
		N-Emis (%)	1.27	10.14	15.59	-0.8	9.61
Apr.	NO$_x$	P-Emis (kt)	52.43	67.17	35.21	39.05	8.72
		N-Emis (%)	8.93	-15.05	-5.22	-7.8	14.59
	NH$_3$	P-Emis (kt)	85.56	90.34	70.52	192.37	56.06
		N-Emis (%)	-3.63	-2.6	-0.18	-1.78	-0.43
	SO$_2$	P-Emis (kt)	33.93	34.44	20.43	110.74	20.2
		N-Emis (%)	-28.14	-0.92	-14.17	-22.97	6.77
	VOC	P-Emis (Mmol)	0.38	0.85	0.23	0.19	0.05
		N-Emis (%)	-28.87	13.71	-25.61	-29.06	-2.29
	PM$_{2.5}$	P-Emis (kt)	1.81	1.96	0.94	1.79	0.62
		N-Emis (%)	-5.12	-3.93	4.34	-8.89	9.54
Jul.	NO$_x$	P-Emis (kt)	50.51	72.03	36.61	41.35	9.01
		N-Emis (%)	-10.62	-29.84	-11.46	-11.94	6.86
	NH$_3$	P-Emis (kt)	108.78	114.78	89.82	245.68	71.16
		N-Emis (%)	-5.41	-2.7	-1.1	-0.9	0.08
	SO$_2$	P-Emis (kt)	35.65	36.95	21.26	115.74	17.51
		N-Emis (%)	-38.45	-4.18	-19.26	-19.71	12.71
	VOC	P-Emis (Mmol)	0.39	0.92	0.24	0.21	0.05
		N-Emis (%)	-22.87	23.85	-21.29	-16.47	8.85
	PM$_{2.5}$	P-Emis (kt)	2.34	3.18	1.06	2.27	0.72
		N-Emis (%)	0.88	-4.94	4.17	-5.4	6.91
Oct.	NO$_x$	P-Emis (kt)	54.83	70.11	37.11	40.84	9.96
		N-Emis (%)	14.56	-19.99	-9.62	-1.5	25.41
	NH$_3$	P-Emis (kt)	50.43	53.4	41.24	110.75	32.28
		N-Emis (%)	-0.53	-4.52	1.54	-3.79	-2.54
	SO$_2$	P-Emis (kt)	35.68	36.08	21.52	116.47	21.74
		N-Emis (%)	-39.8	-2.73	-19.63	-27.43	-2.39
	VOC	P-Emis (Mmol)	0.4	0.89	0.25	0.19	0.06
		N-Emis (%)	-38.33	27.98	-20.39	-34.42	-16.41
	PM$_{2.5}$	P-Emis (kt)	1.94	1.95	1.15	1.85	1.04

N-Emis (%)	0.26	-4.86	3.8	-13.68	9.32

320

3.4 Accuracy Improvements of CTM Simulation for pollutants with N-Emis

We use the CTM to evaluate the accuracy of P-Emis and N-Emis. The configuration of CTM keeps constant.

Generally, simulations using P-Emis tend to underestimate the $PM_{2.5}$ concentrations and overestimate the O_3 concentrations on average of four months in China, which are consistent with our previous studies (Ding et al., 2019; Liu et al., 2019). The

325 underestimation of $PM_{2.5}$ using P-Emis usually appears in Northern and South eastern China, and sometimes occurs in some provinces of the Yangtze River Basin. The simulations of O_3 using P-Emis are generally overestimated at observation sites. Such errors can be narrowed when using N-Emis. We calculated the MAE for each simulation to compare the performances considering all observation sites. After using adjusted emissions (i.e., N-Emis), the MAE for NO_2, SO_2, O_3 and $PM_{2.5}$ concentrations reduced significantly from 7.39 to 5.91 (20.03%), 3.64 to 3.22 (11.54%), 14.33 to 11.56 (19.33%) ppbv and

330 18.94 to 16.67 (11.99%) μg m^{-3}, respectively, average for total 612 observation stations, as shown in Figure 7. Such improvements prove the advantages of using N-Emis compared with P-Emis. Spatial distributions of comparison between simulations and observations in 612 sites can be found in Figure 8. The model performance of most stations has been improved, and a small number of stations with worsen performance show the link between compound pollutants. For example, stations with larger deviations between $PM_{2.5}$ simulation results and observations tend to have greatly improved O_3 performance, and

335 vice versa.
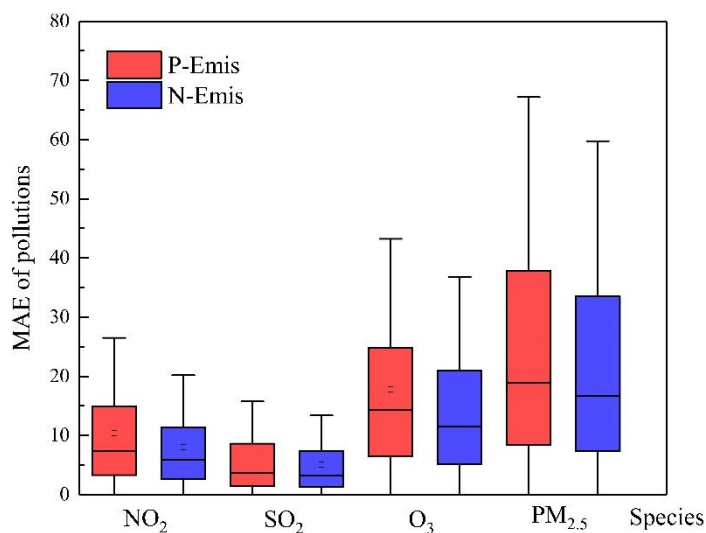
Figure 7. The MAE of NO_2 (ppbv), SO_2 (ppbv), O_3 (ppbv) and $PM_{2.5}$ (μg m^{-3}) concentrations based on P-/N-Emis.
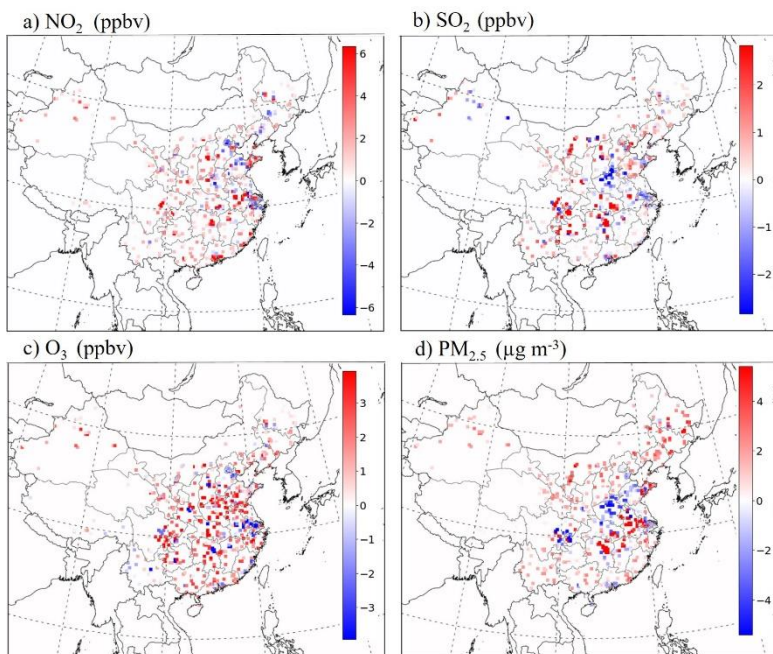
Figure 8: The MAE of NO₂ (ppbv), SO₂ (ppbv), O₃ (ppbv) and PM₂.₅ (μg m⁻³) concentrations based on P-/N-Emis.

Difference of monthly simulations using N-emis & P-Emis as input can be used to estimate the seasonal impacts of emission changes. Concentrations of O_3 and $PM_{2.5}$ tend to increase in July while decrease in other months on average for China. Concentrations of NO_2 and SO_2 tend to decrease in four months, which are consistent with the direct trend of emission adjustments.

We also calculated the average concentrations of four pollutants in five typical regions to quantify the degree of improvement in pollutant concentrations after adjusting the emission inventory, as listed in Table 4. Changes in NO_2 and SO_2 concentrations are consistent with adjustments in emissions but are more sensitive, i.e. a small change (~10%) in emission results in a larger proportional change (~20%) in concentration. The reduced SO_2 emission is an important reason for the improvement of $PM_{2.5}$ overestimations in the Yangtze River Basin. $PM_{2.5}$ concentrations in NWC show the highest increase (15%) compared with other regions. As the emission inventory in NWC has great potential for improvement (subject to production methods and the acquisition of basic data), the qualitative changes in $PM_{2.5}$ concentrations brought about using NN method seem meaningful. The increase and decrease of NO_x and VOC emissions directly control the variance in O_3 concentration. Effect of using N-Emis on O_3 concentration is not obvious, with a change range of less than 5% in typical regions. Although the adjustment ratio of emissions of O_3 precursors is considerable, the O_3 concentration doesn't change by much. The same can be linked to the complex relationship of precursor emissions of NO_x and VOC which might not change simultaneously and in the same direction (e.g. increase NO_x and decrease in VOC or vice-versa) thus resulting in only a slight change in O_3 concentration.

360 **Table 4: Four-month average concentrations of NO₂, SO₂, O₃ and PM₂.₅ in five typical regions using different emission inventories.**

Variables	Version	Regions				
		BTH	YRD	PRD	SCH	NWC
NO_2 (ppbv)	P-Emis	15.69	13.31	6.25	4.82	0.31
	N-Emis	11.85	10.79	5.29	4.45	0.33
SO_2 (ppbv)	P-Emis	6.97	4.32	1.89	4.88	0.26
	N-Emis	5.77	3.95	1.67	3.2	0.37
O_3 (ppbv)	P-Emis	34.79	41.63	40.16	41.94	41.42
	N-Emis	35.51	39.7	38.43	40.06	41.47
$PM_{2.5}$ ($\mu g\ m^{-3}$)	P-Emis	46.28	44.29	22.6	25.96	2.02
	N-Emis	45.28	41.66	22.08	23.71	2.33

4. Conclusion and Discussion

In this study, we pioneer the use of machine learning to re-formulate the problem of emission inventory estimation. It creates a new perspective that the data-driven approach can be applied to automatically improve the quality of the emission inventory, avoiding manual intervention and empirical error. We proposed a differential neural network based chemical transport model (NN-CTM), which achieves a relatively good representation of CTM. And then, we employed backpropagation algorithm to update the emission inventory based on the deviation between observed and NN-CTM predicted pollutant concentrations. In terms of method, we have proposed a novel emission inventory estimation method based on dual learning which consists of dual-loop of emission-to-pollution and pollution-to-emission. Results indicate that our NN based method with adjusted emission inventory performed better than using prior emissions.

Compared with previous studies, our framework employs dual learning mechanism where in the simulated concentrations are compared to ground observation and the gradient is back propagated to update the emission inventory in each epoch. Results show that new emissions after the adjustment can improve the model performance in simulating the concentrations close to observations. The mean absolute error for NO_2, SO_2, O_3 and $PM_{2.5}$ concentrations reduced significantly by 10% to 20%. This application uses a constant biogenic emission inventory, so the potential errors in biogenic emissions are also included in the learning of anthropogenic emissions.

Our method can be naturally extended to other fundamental problems, such as CO_2 and other greenhouse gas emission inventory estimation, and has broad application prospects, such as building a real-time emission monitoring system based on real-time pollutant observation data.

380   **Code/Data availability**

The codes for machine learning are available in https://doi.org/10.5281/zenodo.4607127 (Huang et al., 2021), including demo case for this study with input data from Ding et al. (2016) and the China National Environmental Monitoring Centre (http://beijingair.sinaapp.com/). CMAQv5.2 is an open-source and publicly available model developed by the United States Environmental Protection Agency, which can be downloaded at https://doi:10.5281/zenodo.1167892 (Appel et al., 2018).

385   **Author Contribution**

Lin Huang and Song Liu conceived the research project; Zeyuan Yang analyzed the data; Jia Xing, Jia Zhang, Jiang Bian, Siwei Li, Shuxiao Wang and Tie-Yan Liu provided valuable discussions on research and paper organization; Lin Huang, Song Liu, Zeyuan Yang, Shovan Kumar Sahu, Jia Xing, Jia Zhang and Jiang Bian wrote the paper with contributions from all the authors.

390   **Competing interests**

The authors declare that they have no conflict of interest.

Acknowledgement

This work was supported in part by the National Natural Science Foundation of China (41907190, 51861135102) and the National Key R&D program of China (2017YFC0213005). This work was completed on the "Explorer 100" cluster system of
395   Tsinghua National Laboratory for Information Science and Technology.

References

Aardenne, J. V. and Pulles, T.: Uncertainty in emission inventories: What do we mean and how could we assess it?, 2002.

400 Appel, K., Pouliot, G., Simon, H., Sarwar, G., Pye, H., Napelenok, S., Akhtar, F., and Roselle, S.: Evaluation of dust and trace metal estimates from the Community Multiscale Air Quality (CMAQ) model version 5.0, Geoscientific Model Development, 6, 883-899, 2013.

Appel, K. W., Napelenok, S., Hogrefe, C., Pouliot, G., Foley, K. M., Roselle, S. J., Pleim, J. E., Bash, J., Pye, H. O. T., and Heath, N.: Overview and Evaluation of the Community Multiscale Air Quality (CMAQ)

405 Modeling System Version 5.2, In: Mensink C., Kallos G. (eds) Air Pollution Modeling and its Application XXV. ITM 2016. Springer Proceedings in Complexity. Springer, Cham, doi: https://doi.org/10.1007/978-3-319-57645-9_11, 2018. 69-73, 2018.

Bottou, L.: Large-Scale Machine Learning with Stochastic Gradient Descent, Physica-Verlag HD, 2010.

Brioude, J., Angevine, W. M., Ahmadov, R., and Kim, S.-W.: Top-down estimate of surface flux in the

410 Los Angeles Basin using a mesoscale inverse modeling technique: assessing anthropogenic emissions of CO, NOx and CO2 and their impacts, Atmospheric Chemistry and Physics Discussions, doi: 10.5194/acpd-12-31439-2012, 2012. 2012.

Byun, D.: Science algorithms of the EPA Models-3 community multiscale air quality (CMAQ) modeling system, EPA/600/R-99/030, 1999. 1999.

415 Cho, K., Merrienboer, B. v., Bahdanau, D., and Bengio, Y.: On the Properties of Neural Machine Translation: Encoder-Decoder Approaches, Computer Science, 2014. 2014.

Chung, J., Gulcehre, C., Cho, K., and Bengio, Y.: Empirical Evaluation of Gated Recurrent Neural Networks on Sequence Modeling, Computer Science, 2014. 2014.

Ding, D., Xing, J., Wang, S., Liu, K., and Hao, J.: Estimated contributions of emissions controls,

420 meteorological factors, population growth, and changes in baseline mortality to reductions in ambient PM2.5 and PM2.5-related mortality in China, 2013–2017, Environmental Health Perspectives, doi: 10.1289/EHP4157, 2019. 2019.

Ding, D., Yun, Z., Jang, C., Lin, C. J., Wang, S., Fu, J., and Jian, G.: Evaluation of health benefit using BenMAP-CE with an integrated scheme of model and monitor data during Guangzhou Asian Games, J

425 Environ, 42, 9-18, 2016.

Fan, J., Li, Q., Hou, J., Feng, X., Karimian, H., and Lin, S.: A spatiotemporal prediction framework for air pollution based on deep RNN, ISPRS Annals of the Photogrammetry, Remote Sensing and Spatial Information Sciences, 4, 15, 2017.

Friedl, M. A., Mciver, D. K., Hodges, J. C. F., Zhang, X. Y., Muchoney, D., Strahler, A. H., Woodcock,

430 C. E., Gopal, S., Schneider, A., and Cooper, A.: Global land cover mapping from MODIS: algorithms and early results, Remote Sensing of Environment, 83, 287-302, 2002.

Ghil, M. and Malanotte-Rizzoli, P.: Data Assimilation in Meteorology and Oceanography, Advances in Geophysics, 33, 141-266, 1991.

Guo, S., Hu, M., Zamora, M. L., Peng, J., and Zhang, R.: Elucidating severe urban haze formation in

435 China, Proceedings of the National Academy of Sciences of the United States of America, 111, 17373, 2014.

He, D., Xia, Y., Qin, T., Wang, L., Yu, N., Liu, T.-Y., and Ma, W.-Y.: Dual learning for machine translation, Proceedings of the 30th International Conference on Neural Information Processing Systems, Barcelona, Spain, 820–828, 2016.

440 He, K.: Multi-resolution Emission Inventory for China (MEIC): model framework and 1990-2010 anthropogenic emissions, 2012.

He, K., Zhang, X., Ren, S., and Sun, J.: Deep Residual Learning for Image Recognition, Computer Science, 2015a. 2015a.

He, K., Zhang, X., Ren, S., and Sun, J.: Delving Deep into Rectifiers: Surpassing Human-Level Performance on ImageNet Classification, Computer Science, 2015b. 2015b.

Hochreiter, S. and Schmidhuber, J.: Long Short-Term Memory, Neural Computation, 9, 1735-1780, 1997.

Huang, G., Liu, Z., Laurens, V. D. M., and Weinberger, K. Q.: Densely Connected Convolutional Networks, 2016. 2016.

Huang, L., Liu, S., Yang, Z., Xing, J., Zhang, J., Bian, J., Li, S., Sahu, S. K., Wang, S., and Liu, T.-Y.: The Inventory Optimization Code for Exploring Deep Learning in Air Pollutant Emission Estimation Scale. Zenodo, 2021.

Institute, H. E.: State of global air 2019. Health Effects Institute Boston, M. (Ed.), 2019.

Ioffe, S. and Szegedy, C.: Batch Normalization: Accelerating Deep Network Training by Reducing Internal Covariate Shift, JMLR.org, 2015. 2015.

Kain, J. S.: The Kain–Fritsch convective parameterization: an update, Journal of Applied Meteorology, 43, 170-181, 2004.

Kingma, D. and Ba, J.: Adam: A Method for Stochastic Optimization, Computer Science, 2014. 2014.

Krizhevsky, A., Sutskever, I., and Hinton, G.: ImageNet Classification with Deep Convolutional Neural Networks, 2012.

Li, G.: Report on the completion of environmental conditions and environmental protection targets for 2018, (in Chinese), 2019. 2019.

Liu, S., Xing, J., Westervelt, D. M., Liu, S., Ding, D., Fiore, A. M., Kinney, P. L., Zhang, Y., He, M. Z., and Zhang, H.: Role of emission controls in reducing the 2050 climate change penalty for PM2. 5 in China, Science of The Total Environment, 2020. 144338, 2020.

Liu, S., Xing, J., Zhang, H., Ding, D., Zhang, F., Zhao, B., Sahu, S. K., and Wang, S.: Climate-driven trends of biogenic volatile organic compound emissions and their impacts on summertime ozone and secondary organic aerosol in China in the 2050s, Atmospheric Environment, 218, 117020, 2019.

Mlawer, E., Clough, S., and Kato, S.: Shortwave clear-sky model measurement intercomparison using RRTM, 1998, 23-27.

Mlawer, E. J., Taubman, S. J., Brown, P. D., Iacono, M. J., and Clough, S. A.: Radiative transfer for inhomogeneous atmospheres: RRTM, a validated correlated-k model for the longwave, Journal of Geophysical Research: Atmospheres, 102, 16663-16682, 1997.

Morrison, H., Thompson, G., and Tatarskii, V.: Impact of cloud microphysics on the development of trailing stratiform precipitation in a simulated squall line: Comparison of one-and two-moment schemes, Monthly weather review, 137, 991-1007, 2009.

Pleim, J. E.: A combined local and nonlocal closure model for the atmospheric boundary layer. Part I: Model description and testing, Journal of Applied Meteorology and Climatology, 46, 1383-1395, 2007.

Pleim, J. E. and Xiu, A.: Development and testing of a surface flux and planetary boundary layer model for application in mesoscale models, Journal of Applied Meteorology, 34, 16-32, 1995.

Richter, A., Burrows, J. P., Nüss, H., Granier, C., and Niemeier, U.: Increase in nitrogen dioxide over China observed from space. Nature, Nature, 437, 129-132, 2005.

Ronneberger, O., Fischer, P., and Brox, T.: U-Net: Convolutional Networks for Biomedical Image Segmentation, Computer Science, 2015. 2015.

Sarwar, G., Luecken, D., Yarwood, G., Whitten, G. Z., and Carter, W. P. L.: Impact of an Updated Carbon Bond Mechanism on Predictions from the CMAQ Modeling System: Preliminary Assessment, Journal of Applied Meteorology & Climatology, 47, 3-14, 2008.

Srivastava, N., Hinton, G., Krizhevsky, A., Sutskever, I., and Salakhutdinov, R.: Dropout: A Simple Way to Prevent Neural Networks from Overfitting, Journal of Machine Learning Research, 15, 1929-1958, 2014.

490 Tao, Q., Liu, F., Li, Y., and Sidorov, D.: Air Pollution Forecasting Using a Deep Learning Model Based on 1D Convnets and Bidirectional GRU, IEEE Access, 7, 76690-76698, 2019.

Vallero and Daniel: Translating Diverse Environmental Data into Reliable Information, 2018. 25-41, 2018.

Vesilind, P. A., Peirce, J. J., and Weiner, R. F.: Chapter 18 - Air Pollution, Elsevier Inc., 1988.

495 Wen, C., Liu, S., Yao, X., Peng, L., Li, X., Hu, Y., and Chi, T.: A novel spatiotemporal convolutional long short-term neural network for air pollution prediction, Science of the Total Environment, 654, 1091-1099, 2019.

Wikle, C. K.: Atmospheric modeling, data assimilation, and predictability, 2003. 2003.

Xing, J., Li, S., Ding, D., Kelly, J. T., and Hao, J.: Data Assimilation of Ambient Concentrations of 500 Multiple Air Pollutants Using an Emission-Concentration Response Modeling Framework, Atmosphere, 11, 1289, 2020a.

Xing, J., Li, S., Jiang, Y., Wang, S., Ding, D., Dong, Z., Zhu, Y., and Hao, J.: Quantifying the emission changes and associated air quality impacts during the COVID-19 pandemic in North China Plain: a response modeling study, Atmospheric Chemistry and Physics Discussions, 2020, 1-28, 2020b.

505 Xing, J., Zheng, S., Ding, D., Kelly, J. T., and Hao, J.: Deep Learning for Prediction of the Air Quality Response to Emission Changes, Environmental Science and Technology, XXXX, 2020c.

Xing, J., Zheng, S., Ding, D., Kelly, J. T., Wang, S., Li, S., Qin, T., Ma, M., Dong, Z., Jang, C., Zhu, Y., Zheng, H., Ren, L., Liu, T.-Y., and Hao, J.: Deep Learning for Prediction of the Air Quality Response to Emission Changes, Environmental Science & Technology, 54, 8589-8600, 2020d.

510 Xiu, A. and Pleim, J. E.: Development of a land surface model. Part I: Application in a mesoscale meteorological model, Journal of Applied Meteorology, 40, 192-209, 2001.

Yang, X., Pang, J., Teng, F., Gong, R., and Springer, C.: The environmental co-benefit and economic impact of China's low-carbon pathways: Evidence from linking bottom-up and top-down models, Renewable and Sustainable Energy Reviews, 136, 110438, 2021.

515 Zeiler, M. D., Krishnan, D., Taylor, G. W., and Fergus, R.: Deconvolutional networks, 2010.

Zhang, C., Be Ngio, S., Hardt, M., Recht, B., and Vinyals, O.: Understanding deep learning requires rethinking generalization, 2016.

Zhao, B., Wang, S., Wang, J., Fu, J. S., Liu, T., Xu, J., Fu, X., and Hao, J.: Impact of national NOx and SO2 control policies on particulate matter pollution in China, Atmospheric Environment, 77, 453-463, 520 2013.

Zheng, B., Tong, D., Li, M., Liu, F., and Zhang, Q.: Trends in China's anthropogenic emissions since 2010 as the consequence of clean air actions, Atmospheric Chemistry and Physics, 18, 14095-14111, 2018.

Zheng, H., Zhao, B., Wang, S., Wang, T., Ding, D., Chang, X., Liu, K., Xing, J., Dong, Z., and Aunan, 525 K.: Transition in source contributions of PM 2.5 exposure and associated premature mortality in China during 2005–2015, Environment International, 132, 2019.